The effects of ionizing radiation on the structure and antioxidative and metal binding capacity of the cell wall of microalga Chlorella sorokiniana

DOI:
10.1016/j.chemosphere.2020.127553

Document Version
Accepted author manuscript

Published in:
Chemosphere

The effects of ionizing radiation on the structure and antioxidative and metal-binding capacity of the cell wall of microalga *Chlorella sorokiniana*

Snežana Vojvodić [a], Jelena Danilović Luković [a, b], Bernd Zechmann [c], Mima Jevtović [a, d], Jelena Bogdanović Pristov [a], Marina Stanić [a], Alessandro Marco Lizzul [e], Jon K. Pittman [f], Ivan Spasojević [a, *]

[a] *Department of Life Sciences, Institute for Multidisciplinary Research, University of Belgrade, Kneza Višeslava 1, 11030 Belgrade, Serbia*

[b] *Institute for Application of Nuclear Energy, University of Belgrade, Banatska 31b, 11080 Belgrade-Zemun, Serbia* (present address)

[c] *Center for Microscopy and Imaging, Baylor University, One Bear Place 97046, Waco, TX, USA*

[d] *Faculty of Chemistry, University of Belgrade, Studentski trg 12-16 11001 Belgrade, Serbia* (present address)

[e] *Varicon Aqua, Ball Mill Top Business Park, Unit 12, Hallow, WR2 6PD, UK*

[f] *Department of Earth and Environmental Sciences, School of Natural Sciences, University of Manchester, Michael Smith Building, Oxford Road, Manchester, M13 9PT, UK*

* Corresponding author.

E-mail: redoxsci@gmail.com (I. Spasojević); Tel: +381 11 2078459

Abstract

The impact of ionizing radiation on microorganisms such as microalgae is a topic of increasing importance for understanding the dynamics of aquatic ecosystems in response to environmental radiation, and for the development of efficient approaches for bioremediation of mining and nuclear power plants wastewaters. Currently, nothing is known about the effects of ionizing radiation on the microalgal cell wall, which represents the first line of defence against chemical and physical environmental stresses. Using various microscopy, spectroscopy and biochemical techniques we show that the unicellular alga *Chlorella sorokiniana* elicits a fast response to ionizing radiation. Within one day after irradiation with doses of 1 to 5 Gy, the fibrilar layer of the cell wall became thicker, the fraction of uronic acids was higher, and the capacity to remove the main reactive product of water radiolysis increased. In addition, the isolated cell wall fraction showed significant binding capacity for Cu^{2+}, Mn^{2+}, and Cr^{3+}. The irradiation further increased the binding capacity for Cu^{2+}, which appears to be mainly bound to glucosamine moieties within a chitosan-like polymer in the outer rigid layer of the wall. These results imply that the cell wall represents a dynamic structure that is involved in the protective response of microalgae to ionizing radiation. It appears that microalgae may exhibit a significant control of metal mobility in aquatic ecosystems via biosorption by the cell wall matrix.

Keywords: Alga; Cell wall; Copper; Radiation

1. Introduction

Microalgae are exposed to variable doses of ionizing radiation from natural (*e.g.* radionuclides from soil and rocks), and anthropogenic sources (radioactive waste, radionuclides from mining/ores, nuclear power plant accidents and nuclear testing) (UNSCEAR, 2011). Because photosynthetic microalgae are primary producers of biomass and oxygen, any damaging effects of radiation on these microorganisms will directly impact the function and organization of aquatic ecosystems (Fuma et al., 2012; Nascimento and Bradshaw, 2016). Conversely, microalgae appear to show resilience to radiation stress; for example they are very efficient in the remediation of freshwaters that are contaminated with radioactive metals, such as strontium, uranium, and caesium (Fukuda et al., 2014; Kalin et al., 2005; Vanhoudt et al., 2018). Furthermore, some microalgal species are known to colonize spent nuclear fuel storage pools and uranium tailings pounds showing high levels of radiation and heavy metals pollution (Baselga-Cervera et al., 2018; MeGraw et al., 2018; Rivasseau et al., 2016). Seasonal algal blooms in the spent nuclear fuel storage at Sellafield, UK, is a phenomenon that probably best illustrates the potential of microalgae to adapt to radiation and to thrive in such ecosystems (Foster et al., 2020; MeGraw et al., 2018). It is worth mentioning that these properties demonstrate that microalgae are capable pioneer species in the colonization of highly inhospitable environments (Baselga-Cervera et al., 2018; Rivasseau et al., 2016). Clearly, the effects of ionizing radiation on microalgae and the mechanisms of their adaptation are of fundamental environmental interest, as highlighted recently by the disastrous contamination of water in the Fukushima-Daiichi nuclear power plant accident (Fukuda et al., 2014). It is important to note that high

energy electromagnetic radiation (such as gamma and X) is the most relevant ionizing radiation in aquatic systems. It has high penetrating power, and energy that is sufficient to cause radiolysis of water and to directly oxidize/damage biomolecules (LaVerne, 2000).

It is known that the exposure of microalgae to radiation may result in oxidative damage of lipids and DNA and decreased photosynthetic efficiency, growth and survival (Boreham et al., 1993; Gomes et al., 2017; Rea et al., 2008), as well as in upregulated antioxidative defence and photoprotection, alterations in carbohydrate and general metabolic profile, and other traits of radioresistance (Bradshaw et al., 2019; Foster et al., 2020; Golz and Bradshaw, 2019; MeGraw et al., 2018; Santier et al., 1985). However, the response at the level of the cell wall has not yet been examined. The cell wall is the zone of contact between the microalgal cell and the environment, and the first line of chemical and physical defence (Baudelet et al., 2017). It represents a dynamic multi-layer structure that is actively involved in the adaptation to different stressors (Beacham et al., 2014; Jeong et al., 2017; Yap et al., 2016). Pertinent to this, the cell wall is the main (radio)metal sequestrating (*i.e.* biosorbent) component of microalgal biomass (Hadjoudja et al., 2010; Horikoshi et al., 1979; Vanhoudt et al., 2018). Finally, the thickness and structure of the microalgal cell wall is of technological relevance as it represents a key biological parameter for efficient lipid extraction during microalgal biodiesel production (Anto et al., 2020; Yap et al., 2016). Additionally it is of great relevance as a source of carbohydrates for microalgal bioethanol production (Hernández et al., 2015).

The aim of our study was to determine the effects of ionizing radiation (X-rays) on the cell wall of *Chlorella sorokiniana*. We analyzed: (i) the structure of the cell wall using transmission electron microscopy (TEM) and Fourier-transform infra-red spectroscopy (FTIR); (ii) the capacity of cell wall isolates to remove hydroxyl radical (HO·) using electron paramagnetic resonance (EPR) spin-trapping spectroscopy; and (iii) the capacity of cell wall isolates to bind heavy metals using biochemical assays and EPR. *C. sorokiniana* was selected as a widely used model microalga with high potential for application in industry and wastewater treatment (Lizzul et al., 2018), as it is also commonly found in many freshwater ecosystems.

2. Material and methods

2.1. Cell cultivation

C. sorokiniana (strain CCAP 211/8K; alternative designation UTEX 1230) was obtained from the Culture Collection of Algae and Protozoa, UK. Algal inocula were added to 3N-BBM+V medium; 35 mL in 50 mL Erlenmeyer flasks (TEM experiments), or 150 mL in 250 mL flasks (all other experiments). Initial density in all samples was 5×10^5 cells/mL. Algae were grown for 20 days at 22°C on an orbital shaker (120 rpm) in growth cabinet with a continuous photon flux of 120 µmol m^{-2} s^{-1} (MST TL-D Reflex 36W840 1 SLV/25 tubes, Philips, Amsterdam, Netherlands). At day 20, cultures were in the stationary phase, as determined by optical density (OD_{750} was 7.2 ± 0.5) and biomass (2.0 ± 0.2 mg/mL). The volume of samples was corrected for evaporation at day 20 with sterile deionized water. Samples were irradiated and returned to the growth cabinet for additional 24 h, and then microalgae were collected for further analysis or processing.

2.2. Irradiation protocol

Aliquots of culture (35 mL) were placed in a Petri dish and exposed to X-ray irradiation using CellRad irradiation chamber (Faxitron Bioptics LLC, Tucson, AZ, USA; tube power: 750 W; focal spot size: 1.0 x 1.4 mm; filtration: 1.6 mm Be and 0.5 mm Al; beam angle: 40° divergence; dosimeter: ion chamber). Energy was kept constant at 120 kV; doses and rates were adjusted by changing the current (the doses released by the source were 10, 20 and 50 Gy). Total absorbed doses were 1.09 Gy (rate, 0.25 Gy/min; exposure time 4.4 min), 2.21 Gy (rate, 0.25 Gy/min; 8.9 min), and 5.45 Gy (rate, 0.55 Gy/min; 9.9 min). For simplicity, we refer to these absorbed doses as 1, 2, and 5 Gy. The effects of acute irradiation on cell viability were tested using Evans Blue stain (Sigma-Aldrich, St. Louis, MI, USA), as described previously (Zuppini et al., 2007). Evans Blue is a commonly used measure of cell viability; non-viable cells loose cellular permeability allowing accumulation of the Evans Blue dye, therefore an increased proportion of Evans Blue stained cells in a population indicates an increased proportion of non-vaible cells. The viability is presented as a percentage of Evans Blue negative cells. At least 100 cells were analysed per sample.

2.3. TEM microscopy

Cells were spun down at 5000 g for 5 min, and fixed overnight at 4°C in 0.1 M phosphate buffer (PB; pH 7.2) containing 3% (v/v) glutaraldehyde and 1% (v/v) paraformalaldehyde (Serva, Heidelberg, Germany). Post-fixation was performed with 1% (w/v) osmium tetroxide (Serva) in PB for 2 h at room temperature. Samples were dehydrated in a graded acetone series and then embedded in resin for soft blocks (AGR1031, Agar Scientific, Stansted, UK). Ultra-thin sections (70 µm), obtained with a Leica UC7 ultramicrotome (Leica Microsystems, Wetzlar, Germany), were stained for 15

minutes with 1% uranyl acetate and 5 minutes with 3% lead citrate and observed at 60 kV in a JEOL JEM-1010 TEM (Jeol, Tokyo, Japan). The thickness of cell wall layers was measured using ImageJ (NIH). At least 25 cells with the nuclear mid-section from the control and each irradiation dose treatment were analysed. The thickness of cell wall layers was measured at four points (on the x and y axis of the micrograph with 0 point at the cell's centre).

2.4. Cell wall isolation

Biomass from 150 mL samples (untreated and irradiated with different doses) was spun down and washed 2× in 5 mL distilled water by centrifugation at 2300 g / 5 min. Cell wall isolation was conducted according to the previously described protocol with slight modification (Simonović et al., 2011). Protocol steps were performed at room temperature if not indicated otherwise: (i) homogenization in mortar with liquid N_2 and collection of the sample (~0.5 g fresh weight) with 5 mL water; (ii) 2× wash with 5 mL water by centrifugation at 800 g / 5 min; (ii) 10× shake (15 min) and wash (800 g / 5 min) with 5 mL of chloroform:methanol (1/1 v/v) mixture; (iii) Overnight incubation in the chloroform:methanol solution at 4°C; (iv) shake (1 h) and wash (800 g / 5 min) in 5 mL 1 M NaCl; (iv) shake (1 h) in 5 mL 0.5% Triton and 5× wash (800 g / 5 min) with 5 mL water; (v) shake (20 min) and wash (800 g / 5 min) in 5 mL methanol; (vi) 4× shake (20 min) and wash (800 g / 5 min) in 5 mL acetone; (vii) dry overnight at 30°C; (viii) 2× incubation with 5000 U of amylase (Megazyme, Wicklow, Ireland) per 1 g of sample in PB (pH 7.2) for 24 h at 30°C to remove starch. (ix) wash with 5 mL PB several times until supernatant becomes clear; (x) 2× shake (20 min) and wash (800 g / 5 min) with 5 mL acetone, and leave to dry. The protocol was aimed at preserving the structure of all

160 cell wall polymers (Chen et al., 2000; Hall and Moore, 1983). Gravimetry of isolated cell
161 wall and fresh weight of samples was performed. The composition of the isolated cell
162 wall was analysed by mid-infrared FTIR (4000-400 cm^{-1}) using a Nicolet 6700
163 spectrometer (Thermo Scientific, Waltham, MA, USA). The resolution of spectra was 1
164 cm^{-1}.

165 2.5. Metal-binding capacity

166 Cell wall isolates were tested for capacity to bind Cu^{2+}, Mn^{2+}, and Cr^{3+} ions. Isolates (0.5
167 mg) were placed into 2 mL of 5 mM solutions of $CuCl_2$, $MnCl_2$, or $KCr(SO_4)_2$ (Sigma-
168 Aldrich), that were prepared in 20 mM Hepes buffer (pH 7.5). Samples were vigorously
169 shaken for 10 min in polypropylene tubes (Eppendorf, Hamburg, Germany), and
170 centrifuged at 13000 g / 10 min. Supernatant was collected for biochemical assays,
171 whereas pellet was collected for EPR spectroscopy. The concentration of Cu^{2+} in the
172 supernatant was determined using the fluorescent probe Fura-2 (Sigma-Aldrich), as
173 described previously (McCall and Fierke, 2000), on a FluoroLog 3 fluorimeter (Horiba,
174 Kyoto, Japan) with excitation at 340 nm and emission at 510 nm. Concentrations of two
175 other metals were determined according to previously described colorimetric assays:
176 Mn^{2+} with formaldoxime reagent at λ = 450 nm (Goto et al., 1962), and Cr^{3+} with xylenol
177 orange at λ = 530 nm (Cheng, 1967). Working solutions for calibration curves were
178 prepared daily by stepwise dilution from standard stock solution. Samples were diluted
179 prior to measurements to match the calibration range. The decrease in the
180 concentration of metals in the buffer was used to calculate the binding capacity (µg of
181 bound metal per mg of cell wall isolate).

182 2.6. Antioxidative capacity of the cell wall

183 The capacity of isolated cell wall (0.5 mg in 50 µL water sample) to scavenge $HO^{\cdot}$
184 radical was established using the Fenton reaction, a $HO^{\cdot}$-generating system: Fe^{2+} (1
185 mM; Sigma-Aldrich) + H_2O_2 (3 mM; Carlo Erba Reagents, Milano, Italy), and an EPR
186 spin-trapping method with DEPMPO spin-trap (5-diethoxyphosphoryl-5-methyl-1-
187 pyrroline-N-oxide; Santa Cruz Biotechnologies, Dallas, TX, USA) at the final
188 concentration of 5 mM. Deionized ultrapure 18 MΩ water was used in all experiments.
189 The pH of samples was ~6.5. Spectra were recorded after 2 min incubation at room
190 temperature, using Bruker EMX Nano X-band (9.65 GHz) spectrometer with the
191 following settings: power attenuation, 25 dB; modulation amplitude, 0.2 mT; modulation
192 frequency, 100 kHz; sweep time, 2 min. Antioxidative capacity to remove $HO^{\cdot}$ was
193 calculated using the amplitude (A) of DEPMPO/OH signals according to the following
194 equation: $(A_{Fenton} – A_{Fenton + cell\ wall})/A_{Fenton}$ (Spasojević et al., 2009).

195 2.7. EPR spectroscopy of transition metals

196 Collected pellets (cell wall isolates with bound metals) were placed into 100 µL of Hepes
197 buffer. Samples were vortexed, placed into quartz tubes, and snap-frozen in liquid N_2.
198 Measurements were performed at 77 K on a Bruker EMX Nano spectrometer with finger
199 dewar with liquid N_2, using the following settings: power attenuation, 25 dB; modulation
200 amplitude, 0.8 mT; modulation frequency, 100 kHz; sweep time, 1 min; number of
201 scans/accumulations, 10. Spectra of Cu^{2+}, Mn^{2+} and Cr^{3+} (1.5 mM) in Hepes buffer were
202 recorded for comparison as blanks. Spectrum of Cu^{2+} (1.5 mM) in the presence of
203 chitosan (10 mM) was recorded to analyse interactions with cell wall. Spectral
204 simulations were performed to establish *g*-values and hyperfine splitting (*A*), using
205 Hyperfine Spectrum Software (WF Hagen, TU Delft, The Netherlands) (Hagen, 2008).

206 2.8. Statistics

207 All experiments were performed in three biological replicates, except for the viability test
208 (four replicates) and cell wall isolation (five replicates). Results are presented as mean ±
209 standard error (SE) where appropriate. Statistical significance ($p < 0.05$) in comparison
210 to control experiments was calculated using Mann-Whitney U test.

211 **3. Results**

212 TEM micrographs illustrate the structure of the *C. sorokiniana* cell wall, which is
213 composed of a trilaminar sheath (TLS) and fibrilar wall (Fig. 1a). TLS appears as a
214 translucent line inserted between two electron dense lines; the outer layer (mature
215 mother wall) is separated by an electron translucent space from the thin inner layer
216 (daughter wall). The fibrilar wall is located between the TLS and plasma membrane
217 (Baudelet et al., 2017). The established thickness of the cell wall in untreated *C.*
218 *sorokiniana* is in accordance with data published in the past (Martinez et al., 1991).
219 Irradiation did not induce significant changes in the TLS. On the other hand, the
220 thickness of the fibrilar wall was significantly increased one day after irradiation with 1
221 and 2 Gy (Fig. 1b). In line with this observation, the yield of cell wall was increased by
222 ~50% in irradiated microalgae (Fig. 1c). The slight change in the fibrilar wall following 5
223 Gy of irradiation was not statistically significant. It is noteworthy that there were no
224 significant changes to cell viability in response to irradiation: 90.8 ± 0.7% in controls;
225 84.1 ± 4.1% for algae exposed to 1 Gy; 74.7 ± 1.4% for 2 Gy; and 75.4 ± 1.1% for 5 Gy.
226 Cell wall thickness is an important biological and technological parameter. It provides
227 chemical (including antioxidative) and mechanical protection from the surroundings,
228 determines the carbon budget of the cell, and affects the extractability of lipids and

pigments as well as other industrially-relevant properties of microalgal biomass (Anto et al., 2020; Baudelet et al., 2017; Jeong et al., 2017). The thickening of the cell wall appears to be a common response of microalgae to other types of environmental stress, such as N-deficiency and changes in salinity (in marine algae), under different growing conditions (Beacham et al., 2014; Jeong et al., 2017; Yap et al., 2016). In accord with our findings, the exposure of *Nannochloropsis* to N-stress has been reported to result in the thickening of the inner cellulose-based sheath of a bilayer cell wall (Jeong et al., 2017).

We applied FTIR spectroscopy to analyze the effects of radiation on cell wall composition. FTIR spectra of cell wall isolates showed strong absorption peaks at 3290, 2940, 1645, 1535, 1446, 1385, 1237, 1147, and 1055 cm^{-1} (Fig. 2). The assignation was performed according to available FTIR spectra of microalgal biomass, which mainly reflect the functional groups in the cell wall (Dmytryk et al., 2014; Driver et al., 2015; Hadjoudja et al., 2010; Petrovič and Simonič, 2016). The cell wall composition of *C. sorokiniana* is not fully known. However, available data imply that *Chlorella* cell wall is composed of: (i) a “rigid wall” (sheaths in TLS), which contains glucosamine and N-acetylglucosamine in the form of a chitosan-like polymer; and (ii) a plastic polymeric matrix (fibrilar wall), which is composed of rhamnose, galactose, uronic acids (glucuronic acid in *C. sorokiniana*), arabinose, mannose, and other sugars (Baudelet et al., 2017; Russell, 1995). The band at 3290 cm^{-1} was assigned to glucosamine (N-H stretching), and neutral sugars (O-H and C-O stretching). Bands at 1645, 1535 and 1055 cm^{-1} mainly come from chitosan-like polysaccharides. The 1055 cm^{-1} band was weaker in irradiated samples, which may come from oxidation-induced breakage of

252 polymeric chains (Wasikiewicz et al., 2005). On the other hand, the bands derived from
253 carboxyl and carbonyl groups were stronger in cell wall isolated from irradiated
254 microalgae. This implies that *C. sorokiniana* accumulates uronic acids in the fibrilar wall
255 in response to ionizing radiation. It is noteworthy that no bands corresponding to either
256 phosphoryl or sulfone groups were detected, which is in line with available data on cell
257 wall composition in *Chlorella* (Baudelet et al., 2017). Next we examined the impact of
258 irradiation on the capacity of the cell wall to scavenge $HO^{\cdot}$, the main oxidizing species
259 produced in water radiolysis (LaVerne, 2000). The exposure of *C. sorokiniana* to
260 radiation led to significant increase of antioxidative capacity of the cell wall (Fig. 3). Of
261 note, less intensive spectra stand for more antioxidative capacity. It has been proposed
262 previously that plants 'rely' on non-enzymatic antioxidative defence against $HO^{\cdot}$, such
263 as carbohydrates and cell wall polymers (Bogdanović Pristov et al., 2011; Spasojević et
264 al., 2009). There is no enzymatic system for the removal of this radical. The increased
265 antioxidative capacity could be explained by a higher fraction of uronic acids in the cell
266 wall of irradiated microalgae. A number of studies have found that uronic acid-rich
267 macromolecules, such as xylan (glucuronic acid) and pectin (galacturonic acid), are
268 highly susceptible to reactions with radicals, including $HO^{\cdot}$ (Akhlaq et al., 1990; Fry,
269 1998; Zegota, 2002). We have shown in a comparative study of antioxidative activities
270 of plant cell wall components that pectin and xylan are the most efficient $HO^{\cdot}$
271 scavengers (Bogdanović Pristov et al., 2011). Alternatively, higher antioxidative capacity
272 may be related to radiation-induced fragmentation of chitosan-like polymer. Several
273 studies have reported that such fragmentation results in improved antioxidative
274 performance (Abd El-Rehim et al., 2012; Chmielewski, 2010; Feng et al., 2008; Muley et

al., 2019), which has been related to increased solubility of chitosan fragments compared to high molecular weight polymer (Chmielewski, 2010). The observed increase in cell wall mass and antioxidative capacity represents a fast adaptation mechanism which may explain previous observations that microalgae are less sensitive to chronic than to acute exposure to ionizing radiation (Fuma et al., 2012). Cell wall isolates showed substantial capacity to bind heavy metals (Fig. 4): Cu^{2+}, 0.48 mg/mg; Mn^{2+}, 0.38 mg/mg; and Cr^{3+}, 0.33 mg/mg of cell wall isolate (values for control samples). The irradiation of *C. sorokiniana* culture provoked a significant increase in the capacity of the cell wall to bind Cu^{2+} (Fig. 4a), whereas the capacities for Mn^{2+} and Cr^{3+} binding remained unaltered (Fig. 4b, c). To the best of our knowledge, this is the first report on the metal binding capacity of isolated microalgal cell wall polymers. There are a number of reports of metal binding capacities of intact microalgal biomass (Mehta and Gaur, 2005; Wilde and Benemann, 1993), which were lower than reported in this study. For example, the capacity of *Chlorella vulgaris* biomass for Cu^{2+} binding ranged from 0.01 to 0.19 mg/mg in previous studies (Mehta and Gaur, 2005). Our results are in line with reports identifying cell wall as the main biosorption component of microalgal biomass (Horikoshi et al., 1979; Klimmek et al., 2001; Mehta and Gaur, 2005; Wilde and Benemann, 1993). Further, higher affinity for Cu^{2+} than Mn^{2+} and Cr^{3+} is probably related to differences in coordinative chemistry of these metals. According to the principle of hard and soft acids and bases (HSAB), Cu^{2+} is a borderline acid, whereas Mn^{2+} and Cr^{3+} are hard acids (Hancock and Martell, 1996). This means that they prefer different types of ligands/binding sites within the cell wall. The improvement of Cu^{2+} binding capacity by irradiation may be important for adaptation of microalgae to extreme

298 conditions. Radiological contamination of aquatic ecosystems is usually accompanied
299 by metal pollutants including copper, and vice versa copper mining wastewaters
300 typically show increased levels of radiation (Dessouki et al., 2005; Fuma et al., 2012).
301 Finally, microalgal biomass has been used as biosorbent for remediation of mining,
302 industrial and radioactive wastewaters (Bradshaw et al., 2019; Dessouki et al., 2005;
303 Kaplan, 2013). Our results imply that the application of microalgae in biosorbent
304 technology could be improved by using isolated cell wall material as a sorbent rather
305 than intact cells. However, commercial side of biomass processing has to be evaluated
306 and taken into account.
307 All of the applied metals are paramagnetic so their coordination could be analysed using
308 low-T EPR spectroscopy (Hagen, 2008). Fig. 5 compares EPR spectra of Cu^{2+} in the
309 buffer, bound to cell wall isolates, and bound to chitosan. Cu^{2+} (S =1/2) showed EPR
310 signal with one strong g line and four weak lines coming from hyperfine coupling with
311 $^{63}Cu/^{65}Cu$ nuclei (I = 3/2) along $g_{\|}$. Spectral shape and the rank order of g-values ($g_{\|}$ >
312 g > $g_{\text{free electron}}$), imply that Cu^{2+} is in an octahedral coordination environment with
313 tetragonal distortion in all analyzed systems (Garribba and Micera, 2006). However,
314 hyperfine splittings ($A_{\|}$) and $g_{\|}$ values imply different nature of Cu^{2+} ligands (Peisach and
315 Blumberg, 1974). In the buffer, Cu^{2+} spectrum showed $g_{\|}$ = 2.31 and $A_{\|}$ = 14.7 mT (Fig.
316 5a), which are characteristic for Cu^{2+} bound to 3O and 1N ligands, and in accord with a
317 previous study on Cu^{2+} coordination with Hepes and OH^- ions (Sokołowska and Bal,
318 2005). On the other hand, the spectrum of Cu^{2+} that is bound to the isolated cell wall
319 showed $g_{\|}$ = 2.22 and $A_{\|}$ = 19.0 mT. These values imply that Cu^{2+} is bound to 3N and
320 1O, or to 4N ligands (Fig. 5b). This implies that glucosamine moieties represent the

main sites of coordinate bonding of Cu^{2+} to the cell wall. This is further substantiated by similar $g_{\parallel}$ and $A_{\parallel}$ values for Cu^{2+} that is bound to chitosan-like polymer, which is composed of glucosamine and N-acetylglucosamine (Fig. 5c). Our findings are in line with a previous study that identified amine, secondary amide and carboxyl groups as the most important for Cu^{2+} binding to the surface of *Spirulina* cells (Dmytryk et al., 2014). Amine groups in an electron-withdrawing system (such as glucosamine), as well as secondary amides represent borderline bases and match Cu^{2+} according to HSAB principle (Hancock and Martell, 1996). It is important to point out that spectra did not change notably for the cell wall that was isolated from irradiated algae (Fig. 5b). From these data we can speculate that the increase in Cu^{2+} binding capacity may be the result of increased accessibility to N ligands in damaged/loosened chitosan-like structure in TLS. Pertinent to this, increased binding capacity for uranium in heated biomass of *Chlorella* has been attributed to cell wall denaturation and increased accessibility of binding sites (Horikoshi et al., 1979).

Fig. 6a shows a characteristic six-line spectrum of Mn^{2+} (S = 5/2, I = 5/2) in solution. Cell wall isolates with Mn^{2+} showed similar spectra but of lower intensity (Fig. 6b), which implies that Mn^{2+} was released from the cell wall into the buffer. The remaining bound Mn^{2+} did not show detectable EPR signal. The main reason for this is zero field splitting anisotropy that is promoted by the loss of rapid molecular tumbling, in combination with a large number of transitions, *i.e.* complex multiline spectrum (Ignjatović et al., 2012; Sigel and Sigel, 2000). Empirically, sufficient S/N ratio for the signal of bound Mn^{2+} is achieved when concentration of Mn^{2+} in solution is 10-50-fold lower than bound Mn^{2+} (Sigel and Sigel, 2000), which was not the case here. The EPR results imply that Mn^{2+}

is weakly bound to the cell wall and that irradiation did not alter Mn^{2+} binding capacity, in accordance with the biochemical measurements. Next, Cr^{3+} (S = 3/2) has two nuclear spins: I = 0 (natural abundance of 83%), and I = 3/2 (9.5%) (Azamat et al., 2013). This results in an EPR spectrum containing one strong line for the first isotope, and four weak lines for the latter (Fig. 6c). Similarly to Mn^{2+}, the binding of Cr^{3+} to large slowly-tumbling molecules results in significant line broadening due to zero field splitting anisotropy and fast relaxation (Andriessen and Groenewege, 1976; Hagen, 2008). Line broadening could be also related to paramagnetic effects, *i.e.* dipolar interactions between Cr^{3+} ions that are closely positioned within cell wall matrix (Hagen, 2008; Padlyak et al., 2000). Therefore, no resolved EPR spectrum was obtained for Cr^{3+} that was bound to cell wall (Fig. 6d). The lack of signal of Cr^{3+} in solution means that Cr^{3+} is more strongly bound to the cell wall than Mn^{2+}. This may be related to stronger electrostatic interactions with negative charges on the cell wall for more positive Cr^{3+}.

4. Conclusions

In summary, our results demonstrate that the microalgal cell wall is a dynamic and stress-responsive structure that is involved in fast adaptation to environmental challenges. Within a day after exposure to ionizing radiation, *C. sorokiniana* strengthened its first line of defence against the external environment. The wall became thicker and showed altered composition with increased fraction of uronic acids in the fibrilar layer. The cell wall showed improved capacity to remove the main reactive product of water radiolysis. In addition, the isolated microalgal cell wall exhibited high copper binding capacity, which was further increased by irradiation. These fast adaptation mechanisms are most likely part of a complex process of responses to

different stressors. Knowledge of these responses is essential for the understanding of the ecotoxicology of ionizing radiation and the application of microalgae in metal remediation, wastewater treatment, and biosorbent industry.

Acknowledgment

This work is supported by The NATO Science for Peace and Security Programme, Project number G5320.

References

Abd El-Rehim, H.A., El-Sawy, N.M., Hegazy, S.A., Soliman, S.A., Elbarbary, A.M., 2012. Improvement of antioxidant activity of chitosan by chemical treatment and ionizing radiation. Int. J. Biol. Macromol. 50, 403–413.

Akhlaq, M.S., Schuchmann, H.P., Von Sonntag, C., 1990. Degradation of the polysaccharide alginic acid: a comparison of the effects of UV light and ozone. Environ. Sci. Technol. 24, 379–383.

Andriessen, W.T.M., Groenewege, M.P., 1976. Electron paramagnetic resonance of chromium(III) complexes of the type cis- [Cr(2,2'-bpy)2XY]Z, cis- [Cr(I,IO-phen)2XY]Z, and cis- [Cr(ox)2XY]Z in frozen solutions and powders. Inorg. Chem. 15, 621–625.

Anto, S., Mukherjee, S.S., Muthappa, R., Mathimani, T., Deviram, G., Kumar, S.S., Verma, T.N., Pugazhendhi, A., 2020. Algae as green energy reserve: Technological outlook on biofuel production. Chemosphere 242, 125079.

Azamat, D.V., Dejneka, A., Lančok, J., Trepakov, V.A., Jastrabi, L., Badalayan, A.G., 2013. Pulse-electron paramagnetic resonance of Cr^{3+} centers in $SrTiO_3$. J. Appl. Phys. 113, 174–186.

Baselga-Cervera, B., Romero-López, J., García-Balboa, C., Costas, E., López-Rodas, V., 2018. Improvement of the uranium sequestration ability of a *Chlamydomonas sp*. (ChlSP strain) isolated from extreme uranium mine tailings through selection for potential bioremediation application. Front. Microbiol. 9, 523.

Baudelet, P., Ricochon, G., Linder, M., Muniglia, L., 2017. A new insight into cell walls of *Chlorophyta*. Algal Res. 25, 333–371.

Beacham, T.A., Bradley, C., White, D.A., Bond, P., Ali, S.T., 2014. Lipid productivity and cell wall ultrastructure of six strains of *Nannochloropsis*: Implications for biofuel production and downstream processing. Algal Res. 6, 64–69.

Bogdanović Pristov, J., Mitrović, A., Spasojević, I., 2011. A comparative study of antioxidative activities of cell-wall polysaccharides. Carbohydr. Res. 346, 2255–2259.

Boreham, D.R., Mitchel, R.E.J., 1993. DNA repair in *Chlamydomonas reinhardtii* induced by heat shock and gamma radiation. Radiat. Res. 135, 365–371.

Bradshaw, C., Meseh, D.A., Alasawi, H., Qiang, M., Snoeijs-Leijonmalm, P., Nascimento, F.J.A., 2019. Joint effects of gamma radiation and cadmium on subcellular-, individual- and population-level endpoints of the green microalga *Raphidocelis subcapitata*. Aquat. Toxicol. 211, 217–226.

Chen, M., Sommer, A.J., McClure, J.W., 2000. Fourier transform–IR determination of protein contamination in thioglycolic acid lignin from radish seedlings and improved methods for extractive-free cell wall preparation. Phytochem. Anal. 11, 153–159.

Cheng, K.L., 1967. Spectrophotometric determination of chromium with xylenol orange and methylthymol blue. Talanta 14, 875–877.

Chmielewski, A.G., 2010. Chitosan and radiation chemistry. Radiat. Phys. Chem. 79, 272–275.

Dessouki, T.C.E., Hudson, J.J., Neal, B.R., Bogard, M.J., 2005. The effects of phosphorus additions on the sedimentation of contaminants in a uranium mine pit-lake. Water Res. 39, 3055–3061.

Dmytryk, A., Saeid, A., Chojnacka, K., 2014. Biosorption of microelements by *Spirulina*: towards technology of mineral feed supplements. Sci. World. J. 2014, 356328.

Driver, T., Bajhaiya, A.K., Allwood, J.W., Goodacre, R., Pittman, J.K., Dean, A.P., 2015. Metabolic responses of eukaryotic microalgae to environmental stress limit the ability of FT-IR spectroscopy for species identification. Algal Res. 11, 148–155.

Feng, T., Du, Y., Li, J., Hu, Y., Kennedy, J.F., 2008. Enhancement of antioxidant activity of chitosan by irradiation. Carbohyd. Polym. 73, 126–132.

Foster, L., Muhamadali, H,, Boothman, C., Sigee, D., Pittman, J.K., Goodacre, R., Morris, K., Lloyd, J.R., 2020. Radiation tolerance of *Pseudanabaena catenata*, a cyanobacterium relevant to the First Generation Magnox Storage Pond. Front. Microbiol. 11, 515.

Fry, S.C., 1998. Oxidative scission of plant cell wall polysaccharides by ascorbate-induced hydroxyl radicals. Biochem. J. 332, 507–515.

Fukuda, S.Y., Iwamoto, K., Atsumi, M., Yokoyama, A., Nakayama, T., Ishida, K., Inouye, I., Shiraiwa, Y., 2014. Global searches for microalgae and aquatic plants that can eliminate radioactive cesium, iodine and strontium from the radio-polluted aquatic environment: a bioremediation strategy. J. Plant. Res. 127, 79–89.

Fuma, S., Kawaguchi, I., Kubota, Y., Yoshida, S., Kawabata, Z., Polikarpov, G.G., 2012. Effects of chronic γ-irradiation on the aquatic microbial microcosm: equi-dosimetric comparison with effects of heavy metals. J. Environ. Radioact. 104, 81–86.

Garribba, E., Micera, G., 2006. The determination of the geometry of Cu(II) complexes, J. Chem. Educ. 83, 1229–1232.

Golz, A.L., Bradshaw, C., 2019. Gamma radiation induced changes in the biochemical composition of aquatic primary producers and their effect on grazers. Front. Environ. Sci. 7, 100.

443 Gomes, T., Xie, L., Brede, D., Lind, O.C., Solhaug, K.A., Salbu, B., Tollefsen, K.E.,
444 2017. Sensitivity of the green algae *Chlamydomonas reinhardtii* to gamma radiation:
445 Photosynthetic performance and ROS formation. Aquat. Toxicol. 183, 1–10.
446 Goto, K., Komatsu, T., Furukawa, T., 1962. Rapid colorimetric determination of
447 manganese in waters containing iron: A modification of the formaldoxime method. Anal.
448 Chim. Acta 27, 331–334.
449 Hadjoudja, S., Deluchat, V., Baudu, M., 2010. Cell surface characterisation of
450 *Microcystis aeruginosa* and *Chlorella vulgaris*. J. Colloid Interface Sci. 342, 293–299.
451 Hagen, W.R., 2008. Biomolecular EPR Spectroscopy. CRC Press, Boca Raton.
452 Hall, J.L., Moore, A.L., 1983. Isolation of Membranes and Organelles from Plant Cells.
453 Academic Press, Cambridge.
454 Hancock, R.D., Martell, A.E., 1996. Hard and soft acid-base behavior in aqueous
455 solution. J. Chem. Educ. 73, 654–661.
456 Hernández, D., Riaño, B., Coca, M., García-González, M.C., 2015. Saccharification of
457 carbohydrates in microalgal biomass by physical, chemical and enzymatic pre-
458 treatments as a previous step for bioethanol production. Chem. Eng. J. 262, 939–945.
459 Horikoshi, T,, Nakajima, A., Sakaguchi, T., 1979. Uptake of uranium by various cell
460 fractions of *Chlorella regularis*. Radioisotopes 28, 485–488.
461 Ignjatović, A., Stević, Z., Lavrnić, D., Nikolić-Kokić, A., Blagojević, D., Spasić, M.,
462 Spasojević, I., 2012. Inappropriately chelated iron in the cerebrospinal fluid of
463 amyotrophic lateral sclerosis patients. Amyotroph. Lateral. Scler. 13, 357–362.

464 Jeong, S.W., Nam S.W., Hwangbo, K., Jeong, W.J., Jeong, B.R., Chang, Y.K., Park,
465 Y.I., 2017. Transcriptional regulation of cellulose biosynthesis during the early phase of
466 nitrogen deprivation in *Nannochloropsis salina*. Sci. Rep. 7, 5264.
467 Kalin, M., Wheeler, W.N., Meinrath, G., 2005. The removal of uranium from mining
468 waste water using algal/microbial biomass. J. Environ. Radioact. 78, 151–77.
469 Kaplan, D., 2013. Absorption and adsorption of heavy metals by microalgae, in:
470 Richmond, A., Hu, Q. (Eds), Handbook of Microalgal Culture: Applied Phycology and
471 Biotechnology. John Wiley & Sons Ltd, Hoboken.
472 Klimmek, S., Stan, H.J., Wilke, A., Bunke, G., Buchholz, R., 2001. Comparative analysis
473 of the biosorption of cadmium, lead, nickel, and zinc by algae. Environ. Sci. Technol. 35,
474 4283–4288.
475 LaVerne, J.A., 2000. OH radicals and oxidizing products in the gamma radiolysis of
476 water. Radiat. Res. 153, 196–200.
477 Lizzul, A.M., Lekuona-Amundarain, A., Purton, S., Campos, L.C., 2018.
478 Characterization of *Chlorella sorokiniana*, UTEX 1230. Biology 7, E25.
479 Martinez, F., Ascaso, C., Orus, M.I., 1991. Morphometric and stereologic analysis of
480 *Chlorella vulgaris* under heterotrophic growth conditions. Ann. Bot. 67, 239–245.
481 McCall, K.A., Fierke, C.A., 2000. Colorimetric and fluorimetric assays to quantitate
482 micromolar concentrations of transition metals. Anal. Biochem. 284, 307–315.
483 MeGraw, V.E., Brown, A.R., Boothman, C., Goodacre, R., Morris, K., Sigee, D.,
484 Anderson, L., Lloyd, J.R., 2018. A novel adaptation mechanism underpinning algal
485 colonization of a nuclear fuel storage pond. mBio 9, e02395–e02417.

Mehta, S.K., Gaur, J.P., 2005. Use of algae for removing heavy metal ions from wastewater: progress and prospects. Crit. Rev. Biotechnol. 25, 113–152.

Muley, A.B., Ladole, M.R., Suprasanna, P., Dalvi, S.G., 2019. Intensification in biological properties of chitosan after γ-irradiation. Int. J. Biol. Macromol. 131, 435–444.

Nascimento, F.J.A., Bradshaw, C., 2016. Direct and indirect effects of ionizing radiation on grazer-phytoplankton interactions. J. Environ. Radioact. 155–156, 63–70.

Padlyak, B.V., Kornatowski, J., Zadrozna, G., Rozwadowski, M., Gutsze, A., 2000. Electron paramagnetic resonance spectroscopy of chromium in CrAPO-5 molecular sieves. J. Phys. Chem. 104, 11837–11843.

Peisach, J., Blumberg, W.E., 1974. Structural implications derived from the analysis of electron paramagnetic resonance spectra of natural and artificial copper proteins. Arch. Biochem. Biophys. 165, 691–708.

Petrovič, A., Simonič, M., 2016. Removal of heavy metal ions from drinking water by alginate-immobilised *Chlorella sorokiniana*. Int. J. Environ. Sci. Technol. 13, 1761–1780.

Rea, G., Esposito, D., Damasso, M., Serafini, A., Margonelli, A., Faraloni, C., Torzillo, G., Zanini, A., Bertalan, I., Johanningmeier, U., Giardi, M.T., 2008. Ionizing radiation impacts photochemical quantum yield and oxygen evolution activityof Photosystem II in photosynthetic microorganisms. Int. J. Radiat. Biol. 84, 867–877.

Rivasseau, C., Farhi, E., Compagnon, E., de Gouvion Saint Cyr, D., van Lis, R., Falconet, D., Kuntz, M., Atteia, A., Couté, A., 2016. *Coccomyxa actinabiotis* sp. nov. (*Trebouxiophyceae*, *Chlorophyta*), a new green microalga living in the spent fuel cooling pool of a nuclear reactor. J. Phycol. 52, 689–703.

508 Russell, B., 1995. Determination of Factors Limiting Enzymatic Hydrolysis of the
509 *Chlorella sorokiniana* Cell Wall, PhD Dissertation. University of Florida, Gainesville.
510 Santier, S., Gilet, R., Malaise, E.P., 1985. Induced radiation resistance during low-dose-
511 rate γ irradiation in plateau-phase Chlorella cells. Radiat. Res. 104, 224–233.
512 Sigel, A., Sigel, H., 2000. Metal Ions in Biological Systems: Manganese and Its Role in
513 Biological Processes. Marcel Dekker, New York.
514 Simonović, J., Stevanić, J., Djikanović, D., Salmen, L., Radotić, K., 2011. Anisotropy of
515 cell wall polymers in branches of hardwood and softwood: a polarized FTIR study.
516 Cellulose 18, 1433–1440.
517 Sokołowska, M., Bal, W., 2005. Cu (II) complexation by "non-coordinating" N-2-
518 hydroxyethylpiperazine-N'-2-ethanesulfonic acid (HEPES buffer). J. Inorg. Biochem. 99,
519 1653–1660.
520 Spasojević, I., Mojović, M., Blagojević, D., Spasić, S.D., Jones D.R., Nikolić-Kokić, A.,
521 Spasić, M.B., 2009. Relevance of the capacity of phosphorylated fructose to scavenge
522 the hydroxyl radical. Carbohydr. Res. 344, 80–84.
523 UNSCEAR, 2011. Sources and Effects of Ionizing Radiation. United Nations, New York.
524 Vanhoudt, N., Vandenhove, H., Leys, N., Janssen, P., 2018. Potential of higher plants,
525 algae, and cyanobacteria for remediation of radioactively contaminated waters.
526 Chemosphere 207, 239–254.
527 Wasikiewicz, J.M., Yoshii, F., Nagasawa, N., Wach, R.A., Mitomo, H., 2005.
528 Degradation of chitosan and sodium alginate by gamma radiation, sonochemical and
529 ultraviolet methods. Radiat. Phys. Chem. 73, 287–295.

Wilde, E.W., Benemann, J.R., 1993. Bioremoval of heavy metals by the use of microalgae. Biotechnol. Adv. 11, 781–812.

Yap, B.J.J., Crawford, S.A., Dagastine, R.R., Scales, P.J., Martin, G.J.O., 2016. Nitrogen deprivation of microalgae: effect on cell size, cell wall thickness, cell strength, and resistance to mechanical disruption. J. Ind. Microbiol. Biotechnol. 43, 1671–1680.

Zegota, H., 2002. Some quantitative aspects of hydroxyl radical induced reactions in γ - irradiated aqueous solution of pectins. Food Hydrocoll. 16, 353–361.

Zuppini, A., Andreoli, C., Baldan B., 2007. Heat stress: an inducer of programmed cell death in Chlorella saccharophila. Plant Cell Physiol. 48, 1000–1009.

FIGURE CAPTIONS

Fig. 1. Representative TEM micrographs of *C. sorokiniana* cells and the analysis of cell wall parameters. (a) Characteristic TEM micrographs – controls and cells exposed to different doses of X-ray irradiation in the stationary phase. Analysis was performed one day after the treatment. Cell wall structure shows two main layers: trilaminar sheath – TLS (1) and fibrilar wall (2), see the enlarged area of the cell (dashed line box). (b) Data on thickness of cell wall layers; (c) The yield of cell wall (mass per g of fresh weight (FW). Mean control values (Ctrl) are presented as full line ± SE (dashed line). Statistical significance - * $p < 0.05$.

Fig. 2. FTIR spectra of cell wall isolates from a *C. sorokiniana* stationary phase culture that was untreated (control) or irradiated (2 Gy, similar spectra were recorded for 5 Gy). Circles mark the areas of interest.

Fig. 3. EPR spectra of DEPMPO spin-adduct with $HO^{\cdot}$ that are produced in the absence or the presence of cell wall isolates. (a) Fenton reaction: Fe^{2+} (1 mM) + H_2O_2 (3 mM). Full circle - the amplitude of this peak was used to calculate antioxidative capacity. (b) Cell wall of untreated algae (controls); (c) Cell wall of algae exposed to 1 Gy; (d) Cell wall of algae exposed to 2 Gy; (e) Cell wall of algae exposed to 5 Gy. Antioxidative capacity is presented as mean ± SE. * - statistically significant compared to Fenton reaction ($p < 0.05$).

Fig. 4. The capacity of *C. sorokiniana* cell wall isolates to bind metal ions. (a) Cu^{2+} binding capacity of cell wall polymers from untreated and irradiated microalgae. (b) Mn^{2+} binding capacity. (c) Cr^{3+} binding capacity. Results are presented as means ± SE. Mean

562 control values (Ctrl) are presented as full line ± SE (dashed line). * - statistical
563 significance compared to non-irradiated culture ($p < 0.05$).
564 **Fig. 5.** 77 K EPR spectra of Cu^{2+}. (a) Cu^{2+} (1.5 mM) in Hepes buffer (20 mM; pH 7.5);
565 (b) Cu^{2+} + cell wall isolates from control and irradiated microalgae in the buffer. (c) Cu^{2+}
566 + chitosan. Recording parameters were: power attenuation, 25 dB; modulation
567 amplitude, 0.8 mT; number of scans/accumulations, 10. Gray lines – simulations that
568 delivered the presented *g* and *A* values.
569 **Fig. 6.** 77 K EPR spectra of Mn^{2+} and Cr^{3+}. (a) Mn^{2+} (1.5 mM) in Hepes buffer (20 mM;
570 pH 7.5); (b) Cell wall isolates (from control and irradiated microalgae) that were
571 incubated with Mn^{2+} and placed into the buffer. (c) Cr^{3+} (1.5 mM) in Hepes buffer (20
572 mM; pH 7.5). Arrowheads mark 4 lines of Cr^{3+} with $I = 3/2$. (d) Cell wall isolates (from
573 control and irradiated microalgae) that were incubated with Cr^{3+} and placed into the
574 buffer. Recording parameters were: power attenuation, 25 dB; modulation amplitude,
575 0.8 mT; number of scans, 10.

Figure 1

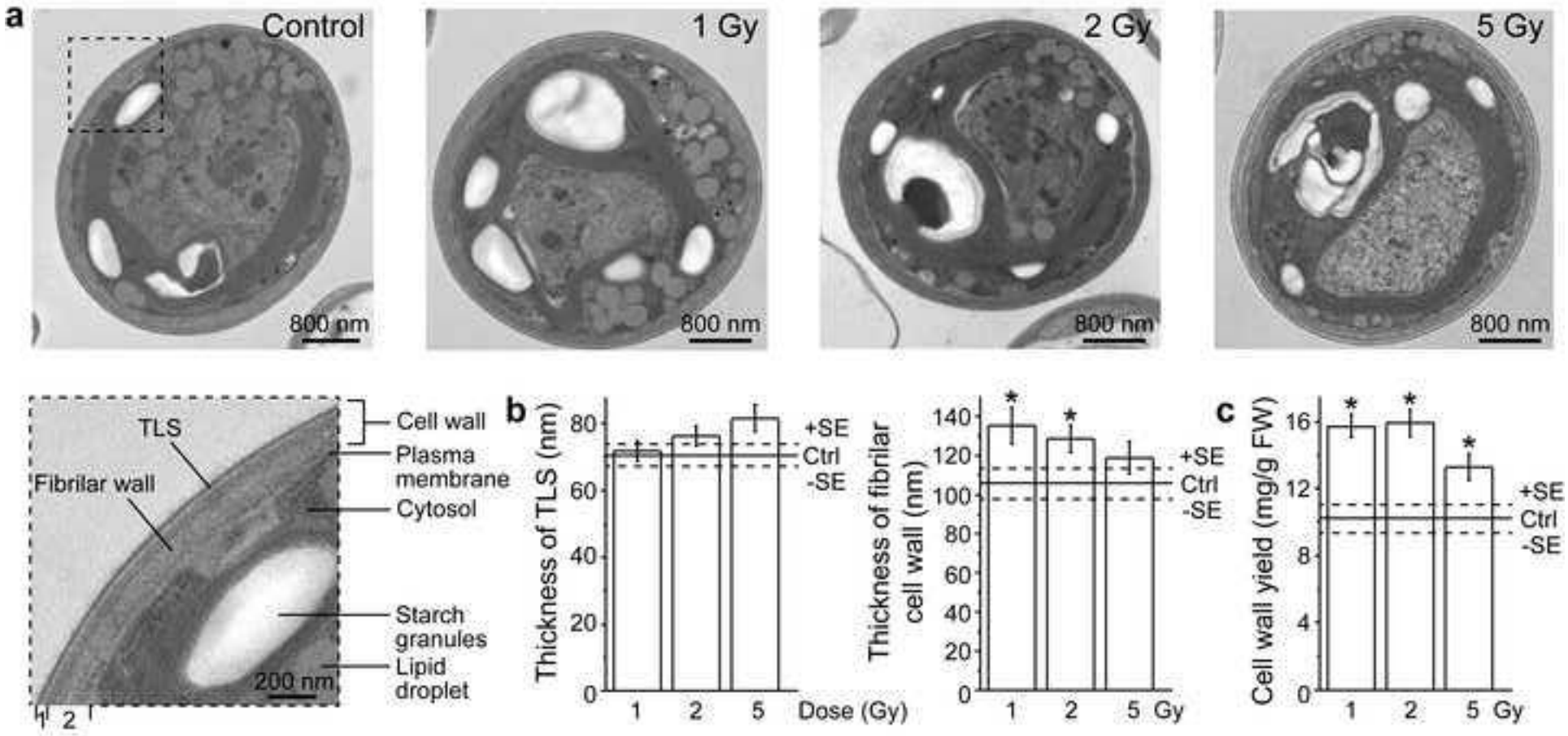

Figure 2

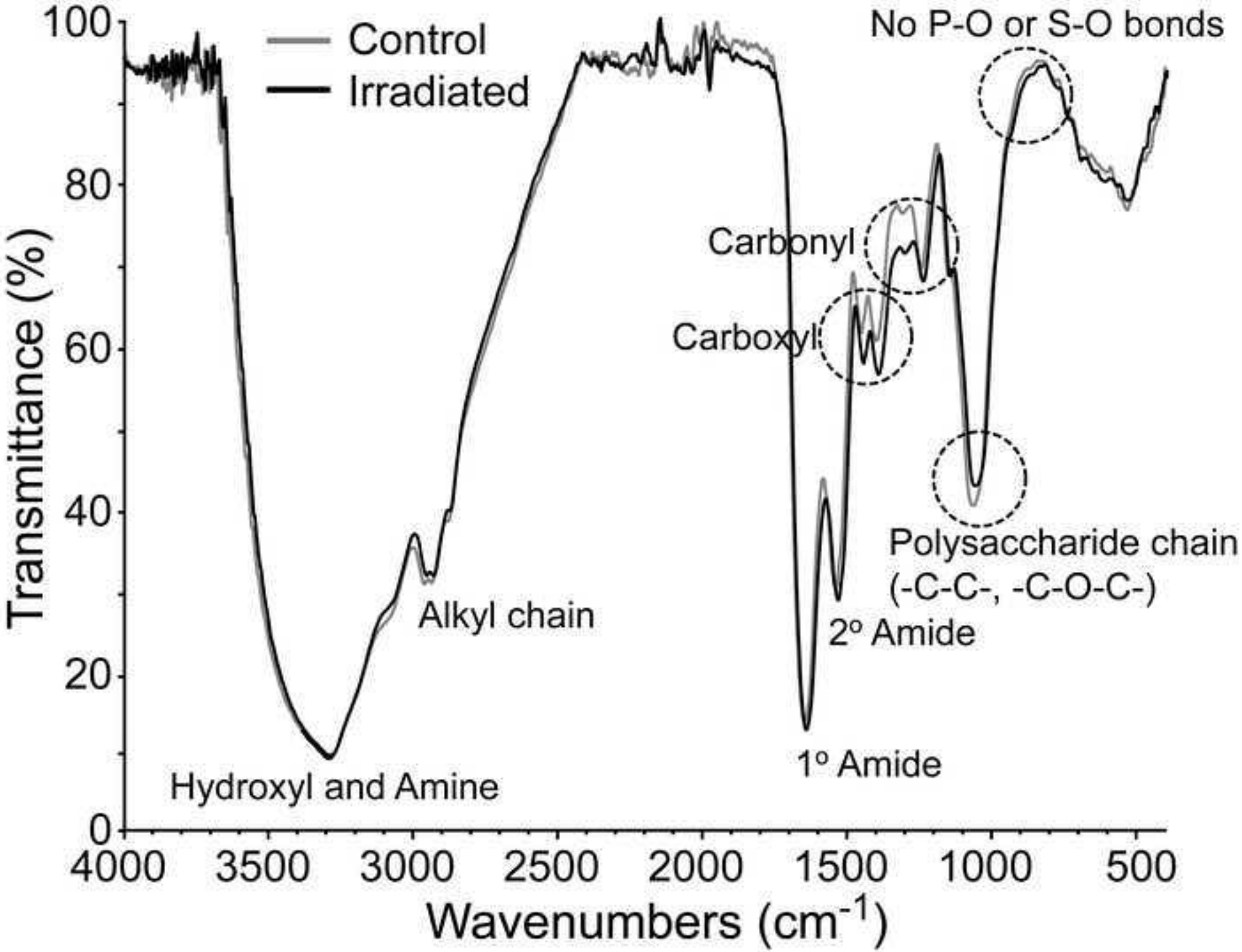

Figure 3

Click here to access/download;Figure;Fig3.tif

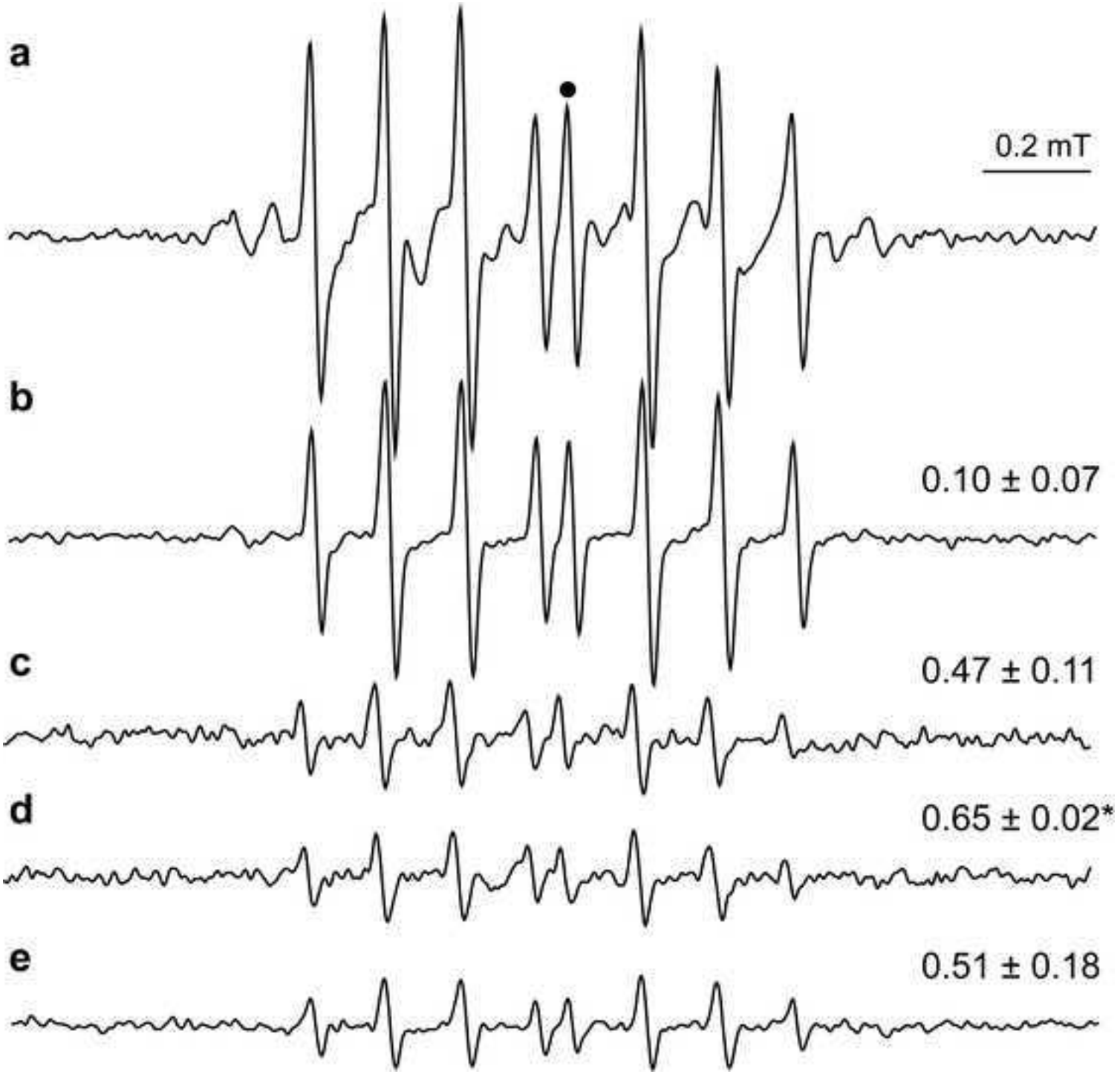

Figure 4

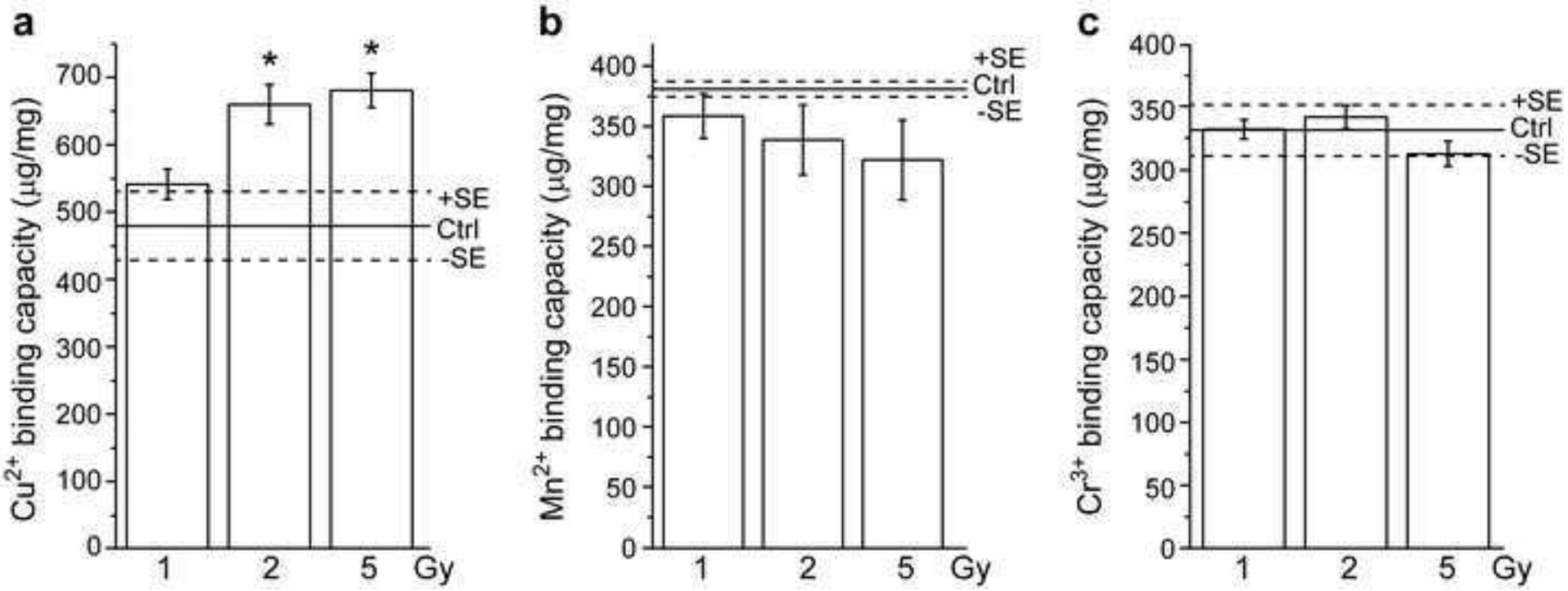

Figure 5

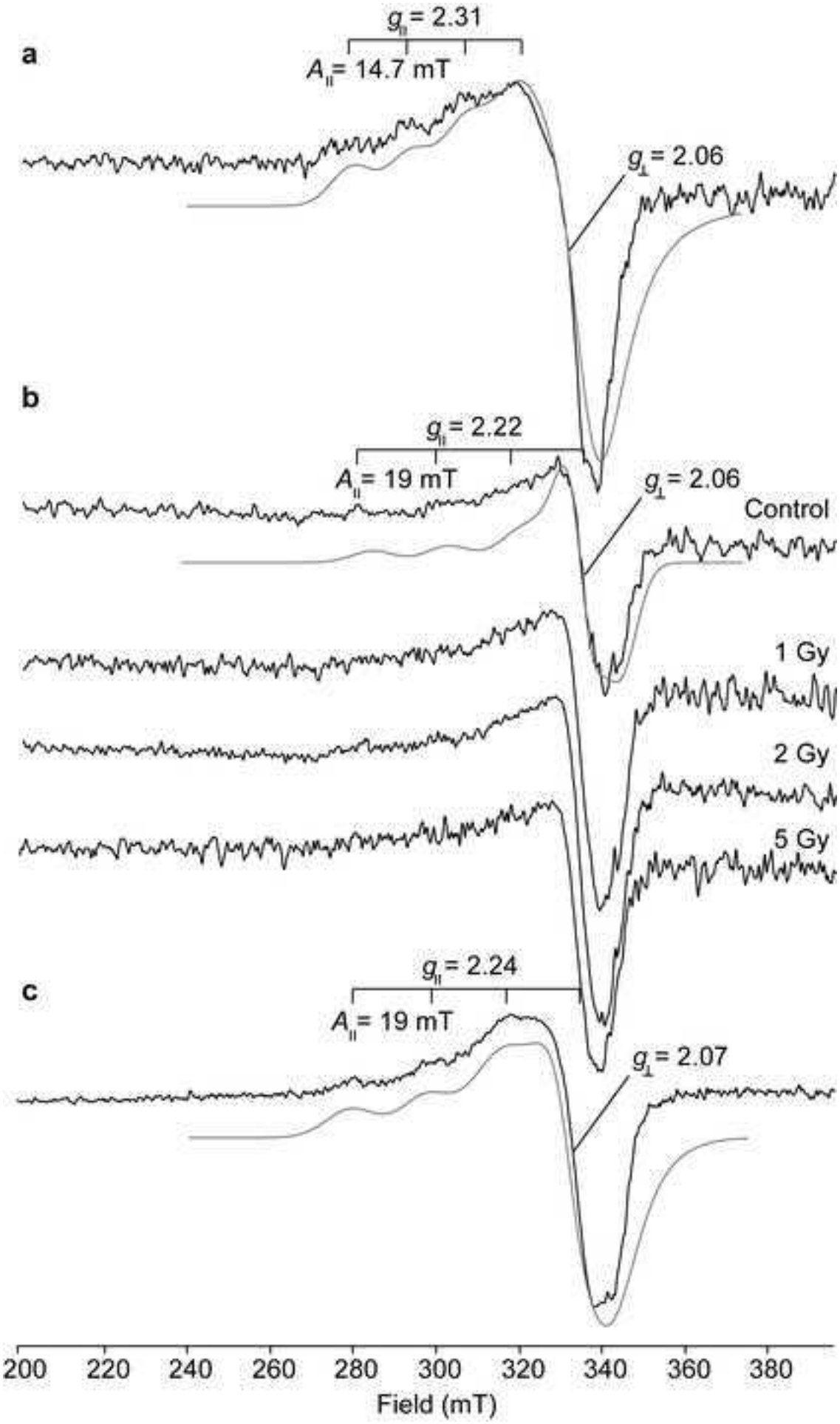

Figure 6